



Contents lists available at ScienceDirect



# Catalysis Today

journal homepage: [www.elsevier.com/locate/cattod](http://www.elsevier.com/locate/cattod)

## Decahedral anatase titania particles immobilized on zeolitic materials for photocatalytic degradation of VOC

I. Jansson<sup>a</sup>, K. Kobayashi<sup>b</sup>, H. Hori<sup>b</sup>, B. Sánchez<sup>a</sup>, B. Ohtani<sup>b</sup>, S. Suárez<sup>a,\*</sup>

<sup>a</sup> CIEMAT, Renewable Energy Division, FOTOAIR: Group of Analysis and Photocatalytic Treatment of Pollutants in Air, Avda. Complutense, 40, 28040, Madrid, Spain

<sup>b</sup> Institute for Catalysis, Hokkaido University, Sapporo 001-0021, Japan

### ARTICLE INFO

#### Article history:

Received 2 July 2016

Received in revised form 6 November 2016

Accepted 21 November 2016

Available online xxx

#### Keywords:

Photocatalysis

Decahedral anatase particles

Zeolites

Adsorbent–Photocatalyst Hybrids

Air treatment

VOC

### ABSTRACT

Decahedral anatase titania particles (DAPs) immobilized on zeolites (zeolite/DAP hybrids), have been prepared by the first time. DAPs have been synthesized from titanium chloride ( $TiCl_4$ ) through a gas-phase reaction process by rapid heating and quenching. DAPs with well-defined  $\{101\}$  and  $\{001\}$  facets were synthesized and dispersed onto the zeolites. The incorporation of an 8wt% of DAPs into the zeolites has been achieved by means of the freezing-drying technique. Two types of zeolites (ZSM-5 and zeolite Y) with different  $SiO_2/Al_2O_3$  contents have been selected as adsorbents. The photocatalytic properties for the degradation of representative volatile organic compounds (VOC), i.e. acetaldehyde, formaldehyde or trichloroethylene were analyzed under batch and continuous flow reactors. Raw materials and composites were characterized by SEM,  $N_2$  adsorption-desorption, UV-vis spectroscopy, XRD, zeta potential and the amount of VOC adsorbed was measured at dynamic conditions. Zeolite/DAP hybrids combine the textural and crystalline properties of zeolite and DAPs phases. The zeolite type (crystal structure,  $SiO_2/Al_2O_3$  ratio and surface net charge) play a relevant role in the dispersion of DAPs. Zeolite/DAP composites show better photocatalytic performance than those prepared with commercial  $TiO_2$  due to the presence of  $\{001\}$  facets in the former. The composites prepared with hydrophobic ZSM-5 and DAPs, are the most versatile materials for photooxidation of aldehydes and organochloride compounds, with substantially less formation of non-desirable reaction products respect to those based on benchmark  $TiO_2$ .

© 2016 Elsevier B.V. All rights reserved.

## 1. Introduction

Heterogeneous photocatalysis is one of the most promising technologies for air decontamination [1].  $TiO_2$  is the main semiconductor component used as photocatalyst because is a non-toxic, abundant and inexpensive material endowed with high photocatalytic efficiency and chemical stability [2]. Despite these properties,  $TiO_2$  still presents limitations affecting its photocatalytic performance. On one hand, it is only active under UV light, and therefore it can only use about a 5% of the total solar radiation spectrum [3]. On the other hand, when the activation of the photocatalyst occurs, a high fraction of the electrons promoted from the valence band to the conduction band become recombined, reducing the photocatalytic efficiency greatly [4]. In this regard, it has been reported that the recombination process occurs at grain boundaries and crystalline defects. Therefore, the synthesis of crystalline

$TiO_2$  particles with a low density of defects is a promising strategy to improve the photocatalytic performance [5]. It is reported in the literature that  $TiO_2$   $\{001\}$  facets are more reactive towards the dissociative adsorption of reactant molecules than  $\{101\}$  ones [6,7]. Decahedral anatase titania particles (DAPs) exhibit a high fraction of  $\{101\}$  facets along with two additional square  $\{001\}$  facets. As a result, DAPs show a great potential as photocatalysts for the degradation of organic pollutants [5,8]. The preparation of DAPs can be performed by hydrothermal reactions using fluorine species as shape-control reagents [9–11]. The drawback of this method, however, is the strong adsorption of the shape-control reagents at the surface of the synthesized particles which severely affects the photodegradation efficiency [12]. To synthesize anatase  $TiO_2$  crystals with  $\{001\}$  facets without using fluorine species, the crystal growth should to be confined within the kinetically controlled regime under non-equilibrium conditions. These conditions can be achieved by conducting the synthesis at high-temperature using rapid heating and quenching processes in gas-phase reaction [13].

Adsorbent–photocatalyst hybrid materials (APHs), are bifunctional materials based on the combination of an adsorbent and a

\* Corresponding author.

E-mail address: [silvia.suarez@ciemat.es](mailto:silvia.suarez@ciemat.es) (S. Suárez).

semiconductor. These materials have demonstrated enhanced photocatalytic properties for the degradation of pollutants in air [14]. By combining the individual properties of both materials, a synergistic effect is developed during the photocatalysis with AHPs [15,16]. Thus, the adsorbent captures the pollutants and facilitate their transport to the interface with the semiconductor phase. The appropriate combination of the properties of both materials allows an improvement in the photocatalytic performance. An increase in the reaction rate along with a decrease of the formation of secondary products, i.e., higher degree of mineralization, has been reported in the literature [14]. When the semiconductor is combined with the adsorbent, an improvement in the textural properties of the final material, this is, higher BET area and pore volume is usually reported [17–19]. Moreover, depending on the physico-chemical properties of the adsorbent, the promotion of the electron-hole separation, the incorporation of hydroxyl species, the control of the deactivation processes or the absorption of visible light, can be promoted. Finally, adsorbents can also act as binders providing optimal rheological properties, allowing the formation of shaped materials and facilitating the separation of the photocatalyst from the fluid [19]. Zeolites are microporous aluminosilicates-based materials commonly used as commercial adsorbents and catalysts. These aluminosilicates are characterized by high crystallinity, large surface area, high adsorption capacity, acidity and shape selectivity [20–22]. These properties place zeolites as ideal adsorbents to improve the photoefficiency of TiO<sub>2</sub> for the degradation of pollutants.

The photocatalytic properties of zeolites/TiO<sub>2</sub> hybrids have been already published in the literature [23–26]. Also, studies related to the synthesis and features of DAPs are numerous [8,12,13,27]. Nevertheless, to our knowledge, the effect of the addition of small amounts of decahedral anatase particles to zeolitic structures has not been reported hitherto. Moreover, most of the photocatalytic results reported in the literature concerning the photocatalytic performance of DAPs are obtained in batch reactor where a fix amount of the pollutant is introduced in the reactor and forced to react with the photocatalyst [12,13]. Long residence times are generally required for the complete removal of the pollutant. However, these reaction conditions are far from real applications, where the contact time between the pollutant and the photocatalyst active sites is short and treatment of a high gas volume is required.

In this study, decahedral anatase titania particles were prepared by a gas-phase process using TiCl<sub>4</sub> as a precursor and immobilized on zeolites for the abatement of VOC in gas phase. These hybrids, hence forward referred to as zeolite/DAP hybrids were prepared by the freezing drying technique. Furthermore, zeolite/TiO<sub>2</sub> composites based on commercial TiO<sub>2</sub> were prepared for comparison purposes. The photocatalytic properties of the synthesized materials for the degradation of aldehydes (acetaldehyde and formaldehyde), common pollutants of indoor air and an organochloride compound such as trichloroethylene, were evaluated in bath and in a continuous flow reactor at low contact time. The influence of the adsorption ability, the textural properties, the nature of the VOC molecule and the zeolite type (zeolite Y vs. ZSM-5) in the physico-chemical and photocatalytic properties was investigated.

## 2. Experimental

### 2.1. Synthesis of decahedral anatase titania particles

Decahedral anatase titania particles (DAPs) were prepared by a gas-phase process in a quartz tubular reactor using titanium(IV) chloride (TiCl<sub>4</sub>) as the TiO<sub>2</sub> precursor. Liquid TiCl<sub>4</sub> (2.5 mL h<sup>-1</sup> during 3 h) was conducted into a vaporizer vessel where argon

(75 mL min<sup>-1</sup>, 180 °C) was introduced as the carrier gas for TiCl<sub>4</sub> vapor. Then, Ar/TiCl<sub>4</sub> gas and oxygen (800 mL min<sup>-1</sup>) preheated to a fixed temperature, were mixed in the reaction zone of the quartz reactor heated and the oxidation reaction takes place, according to Eq. (1).



The part of the reactor heated was wrapped with a platinum foil into an infrared furnace at 1,200 °C. Once the reaction was finished, the reactor was rapidly quenched. Then, the DAPs synthesized were collected by filtration and washed [8]. Finally, water was removed by freeze-drying under vacuum for 24 h (EYELA Freeze Dryer FDU-2100, P < 10 Pa, T = -80 °C).

### 2.2. Preparation of zeolite/TiO<sub>2</sub> hybrids

Five types of commercial zeolites from Zeolyst, two zeolites Y with the FAU structure and SiO<sub>2</sub>/Al<sub>2</sub>O<sub>3</sub> ratio 5–80 (CBV 600 and CBV 780) and three ZSM-5 with the MFI structure and SiO<sub>2</sub>/Al<sub>2</sub>O<sub>3</sub> ratio 23–280 (CBV 2314, CBV 8014 and CBV 28014), were selected as adsorbents.

The incorporation of TiO<sub>2</sub>-DAPs onto the zeolite was performed by means of the freezing-drying technique. 160 mg of DAP were added to a suspension of 2 g of zeolite in water and the mixture was stirring for 2 h. Next, the suspension was frozen with liquid N<sub>2</sub> and water was removed by freezing-drying under the same conditions as described in the previous section. In agreement with previous studies conducted with zeolite/TiO<sub>2</sub> hybrids wherein the optimum mass of zeolite and titanium was evaluated for the maximum photocatalytic performance, the amount of TiO<sub>2</sub> was set at 8 wt%. [18].

Commercial photocatalyst TiO<sub>2</sub> (G5, Millenium/Cristal) was used as a reference sample. The hybrids materials were prepared by mechanical mixing of the commercial titania and the zeolites in nitric acid. Then, the samples were extruded and treated thermally at 500 °C for 3 h.

### 2.3. Characterization techniques

Brunauer-Emmett-Teller (BET) specific surface area and pore volume of the samples was determined from nitrogen adsorption at -196 °C in a Micrometrics Asap 2020 Analyser. Samples were outgassed overnight at 120 °C and pressure < 1.66 10<sup>2</sup> Pa. Micropore volume and sizes were estimated by N<sub>2</sub> adsorption at low partial pressure range ( $P/P_0 = 0\text{--}0.1$ ) using the Horvath-Kawazoe (H-K) method and the Saito and Foley approximation for cylindrical pore geometry. Crystalline and non-crystalline composition of samples was analyzed by powder X-ray diffraction (PXRD) using a Rigaku SmartLab diffractometer with CuK $\alpha$  radiation operating at 40 kV and 30 mA. NiO (0.050 g, Wako Pure Chemical) was selected as an internal standard and mixed with 0.200 g of sample. Bragg's angle between 10 and 80° were recorded at scanning rate of 1.0° min<sup>-1</sup> and step of 0.008°. The acquired diffractograms were analyzed using the software installed in the controlling personal computer (PDXL including a RIETAN-FP Rietveld analysis package). On the assumption that NiO is 100% crystalline, i.e., without non-crystalline part, crystalline anatase and rutile contents were calculated based on the results of Rietveld analysis [28]. Zeta potential measurements were performed with a Zetasizer Nano ZS90 with a MPT-2 autotitrator. Experiments were carried out using 15 mg of 1 μm powder samples suspended in 100 mL of 10<sup>-3</sup> M KCl solution, adjusting the pH value with 0.2 M and 0.02 M KOH and HCl solutions. Each curve was recorded at least three times to ensure reproducibility. The Diffuse reflectance spectra of the solids were obtained using a UV-vis/DRS technique on a JASCO V-670 spectrophotometer equipped with a PIN-757 integrating sphere

accessory for diffuse reflectance spectra acquisition. The reflectance data was converted with the Kubelka-Munk equation to absorption coefficient  $F(R_\infty)$  and the band gap energy was evaluated by the Tauc plot [29]. The morphology of DAP and the dispersion of the DAP on the zeolites were investigated by scanning electron microscopy JEOL JSM-7400F at 5 kV.

#### 2.4. Photocatalytic activity tests and adsorption ability

The photocatalytic activity of the DAPs and the APHs for the degradation of three VOC molecules, namely acetaldehyde (AcH), formaldehyde (FMD) or trichloroethylene (TCE) was measured in air under UV-A irradiation conditions.

The photodegradation of acetaldehyde was evaluated in a batch reactor consisting of a cylindrical Pyrex glass vessel sealed with a septum (114 mL, 120 mm length and 35 mm diameter). The materials (80 mg) were supported on a borosilicate glass roughened slide. Previous the photocatalytic test, samples were pretreated with UV-A light during 12 h. Gaseous acetaldehyde (4.67  $\mu\text{mol}$ ) was injected into the chamber filled with ambient air. The AcH concentration in the reactor was of 1,000 ppm. Once acetaldehyde was completely adsorbed on the material at dark conditions (ca. 240 min), the samples were irradiated with UV black light (fluorescent GE/Hitachi FL10BL-B 10W), 1  $\text{mW cm}^{-2}$  irradiance for 60 min. The evolution of the amount of AcH reacted and  $\text{CO}_2$  produced in the reaction were measured by GC-FID (Shimadzu GC-14B) using a Phenomenex ZB-WAX column in the former and a GC equipped with a methanizer and a Porapak-Q column in the later [30].

The photocatalytic performance for the oxidation of FMD and TCE was studied in a continuous flow reactor. The flat photoreactor was made of stainless steel (external dimensions: 120 mm x 50 mm x 10 mm) except for one size where a borosilicate glass window (37  $\text{cm}^2$ ) was placed. The samples (30 mg) were immobilized on a borosilicate glass slide and place inside the reactor. The materials were pre-treated during 12 h under air atmosphere and UV-A irradiation in order to remove water and weakly adsorbed organic molecules at the surface. A gas mixture of TCE or FMD with air was prepared using gas cylinder of  $\text{C}_2\text{HCl}_3/\text{N}_2$  (Air Liquide, 70 ppm) or  $\text{HCHO}/\text{N}_2$  (50 ppm) and compressed air free of water and  $\text{CO}_2$ . The flow rate was controlled by using electronic mass flow controllers. The photocatalytic tests were performed using two UV lamps (Philips TL8 Actinic BL) with a maximum emission at 365 nm. The irradiance at the photocatalyst surface was 6.5  $\text{mW cm}^{-2}$ . The photocatalytic performance was evaluated varying the total air gas flow between 500 and 900  $\text{mL min}^{-1}$  (residence time 0.77–0.43 s) with a FMD or TCE concentration of 15 ppm and 25 ppm, respectively. The gas-phase composition was continuously monitored by a FTIR spectrometer (Thermo Nicolet 57000) equipped with a temperature controlled multiple reflection gas cell optical path 2 m [31]. The adsorption ability of the zeolite/DAP samples was studied at dynamic conditions in same experimental system using for the photodegradation of FMD and TCE as described elsewhere. The experiment at the batch conditions were repeated seven times to ensure reproducibility of the results. On the other hand, due to the stability of the operating conditions at the continuous flow reactor, experiments were repeated two times.

### 3. Result and discussion

#### 3.1. Characterization of zeolite/TiO<sub>2</sub>-DAPs samples

**Table 1** collates the main textural properties of the commercial TiO<sub>2</sub>, DAPs, zeolites and the zeolite/DAP hybrids. The pore diameter, pore volume and specific surface area were determined using N<sub>2</sub> adsorption-desorption isotherms. Zeolites Y present a BET area

between 600 and 800  $\text{m}^2 \text{g}^{-1}$  with pore size of 0.75 nm. On the other hand, ZSM-5 showed lower BET area than zeolite Y, ranging around 300–400  $\text{m}^2 \text{g}^{-1}$  and 0.5 nm mean pore size. The zeolites exhibit the typical profile for type I isotherms, characteristic of microporous materials with a hysteresis H4 indicative of slit-shaped pores, in accordance with the IUPAC classification [32]. These data fits with those found in the literature, for similar FAU and MFI zeolite structures [33]. DAPs present lower surface area than that of commercial TiO<sub>2</sub>, with mesoporosity mainly generated due to interparticular separation. The specific surface area of the TiO<sub>2</sub>-DAPs can be controlled by varying the TiCl<sub>4</sub> concentration in the feed gas during the synthesis step. In a previous study, Sugihara et al., reported that the photocatalytic activity of TiO<sub>2</sub>-DAPs varies with the surface area being maximum for the catalyst with a BET area of 12  $\text{m}^2 \text{g}^{-1}$  [13]. As a consequence, we have synthesized similar particles following that synthetic approach for this study. Taking into account that the zeolite is the main component (92wt%) of the zeolite/DAP composites, the textural properties of zeolites determine the properties of the composites. The textural properties of the hybrids prepared with commercial TiO<sub>2</sub> are similar to the ones of the zeolite/DAPs but with a slight large BET area and porosity values due to the inherent properties of TiO<sub>2</sub>-G5.

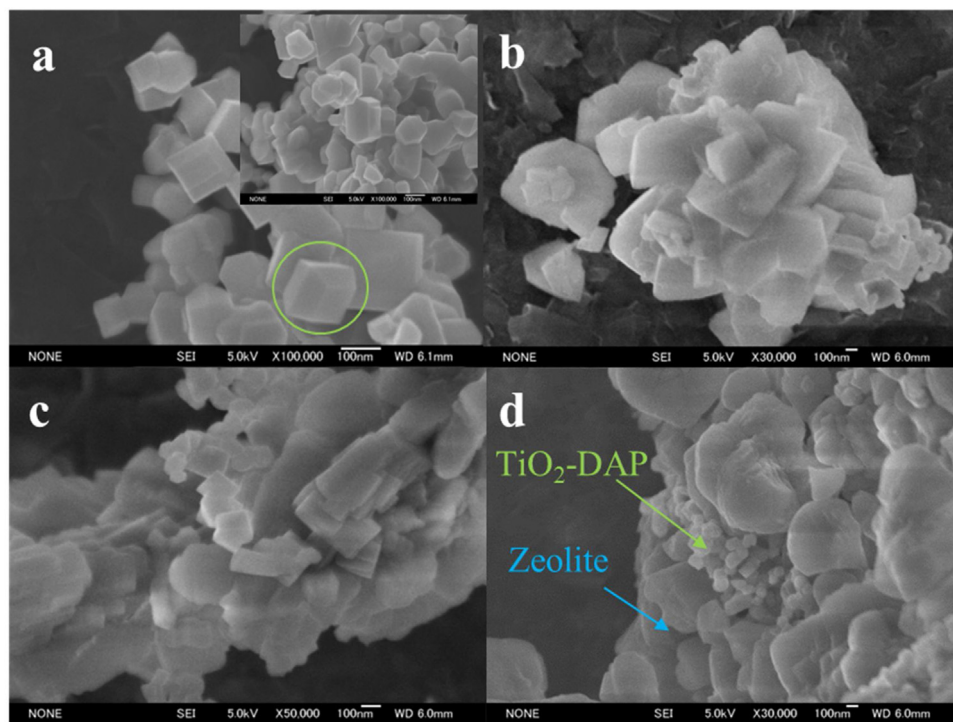
The adsorption ability of the raw materials and the hybrids towards different VOCs molecules was studied under dynamic conditions (**Table 1**). Commercial zeolites exhibit high adsorption capacity for CH<sub>3</sub>CHO and HCHO. However, the organochloride adsorption ability is lower as compared to the aldehydes. The zeolites with unbalanced sites or electrostatically polarised are especially relevant for the adsorption of polar molecules, due the formation of strong adsorption sites [34,35]. The adsorption of the three model molecules under study on the zeolite/DAP composites, independently of the nature of the zeolite (MFI or FAU structure) follows the same pattern: the higher the SiO<sub>2</sub>/Al<sub>2</sub>O<sub>3</sub> ratio, the lower the adsorption ability. The presence of Al-OH, Si-O-Al or Al-O-Al surface groups promotes the adsorption of the organic compounds. It is well established that the SiO<sub>2</sub>/Al<sub>2</sub>O<sub>3</sub> ratio defines the hydrophilic-hydrophobic character of zeolites and their sorptive properties [25,36,37]. In spite of the lower surface area of the DAPs (14  $\text{m}^2 \text{g}^{-1}$ ), the results show an unexpected high adsorption ability for aldehydes, especially acetaldehyde. In the case of TiO<sub>2</sub>, the amount of aldehyde adsorbed is somehow related to the surface area of the materials. Noguchi et al. found differences between the decomposition rates of formaldehyde and acetaldehyde and ascribed them to differences in their adsorption strengths [38]. On the other hand, the ability of TiO<sub>2</sub> to adsorb TCE is low and this molecule tends to become adsorbed on microporous materials especially in MFI structures, with 0.5 nm mean pore size. Finally, the mixture with an 8wt% DAPs, combine the individual properties of the raw materials, resulting in a diminution of the BET area of the composites, the blocking of a small portion of the micropores and a modification of the amount of VOC adsorbed.

The DAPs and zeolite/DAP samples were analyzed by scanning electron microscopy. **Fig. 1a** shows SEM images of DAPs with a mean particle size around 100 nm. As observed in the micrograph, pure decahedral particles are the most abundant particles (marked with a green circle). However, particles exhibiting decahedral shape but with noticeable defects on the facets, (e.g., mounds in the {001} facets), aggregates and broken decahedral particles and others particles with a shape different from decahedral geometry (regular or irregular) can be also observed as previously reported [8]. Particles with mounds or deposits on the {001} facets were detected (see **Fig. 1a** inset). The appearance of this type of morphology depends on the synthesis conditions. Shorter reaction time at lower temperatures with concentrated titania favors the formation of mound in the {001} facets. The formation of new crystals on the surfaces

**Table 1**

Properties of raw materials and zeolite/DAP hybrids at room temperature.

Sample	Material	SiO <sub>2</sub> /Al <sub>2</sub> O <sub>3</sub> <sup>a</sup>	BET Area m <sup>2</sup> g <sup>-1</sup>	V <sub>p</sub> <sup>b</sup>			Mean pore size		Adsorption		
				V <sub>T</sub>	micro	meso	micro	meso	CH <sub>3</sub> CHO	HCHO	C <sub>2</sub> HCl <sub>3</sub>
<i>Raw materials</i>											
TiO <sub>2</sub> -DAP	TiO <sub>2</sub>	-	14	0.17	-	0.17	-	100	773	443	12
TiO <sub>2</sub> -G5 <sup>c</sup>	TiO <sub>2</sub>	-	152	0.39	-	0.26	-	7/13	973	1,940	18
Z1	-	5	607	0.35	0.25	0.10	0.74	10	799	882	150
Z2	-	80	826	0.48	0.36	0.12	0.75	17	279	319	127
Z3	-	23	352	0.18	0.14	0.04	0.51	-	3,332	4,051	522
Z4	-	50	447	0.26	0.18	0.08	0.55	-	584	803	481
Z5	-	280	402	0.26	0.13	0.03	0.60	-	201	473	453
<i>Zeolite/DAP Hybrids</i>											
Z1/DAP	Zeolite Y	5	476	0.34	0.21	0.14	0.74	10	568	92	113
Z2/DAP	Zeolite Y	80	725	0.50	0.28	0.22	0.75	15	205	28	30
Z3/DAP	ZSM-5	23	298	0.18	0.13	0.05	0.51	-	2,212	3,906	470
Z4/DAP	ZSM-5	80	377	0.26	0.14	0.12	0.55	-	768	784	373
Z5/DAP	ZSM-5	280	392	0.18	0.14	0.04	0.60	-	258	318	327

<sup>a</sup> SiO<sub>2</sub>/Al<sub>2</sub>O<sub>3</sub> mole ratio.<sup>b</sup> V<sub>p</sub>: pore volume obtained for N<sub>2</sub> adsorption-desorption isotherm.<sup>c</sup> Data obtained for sample heat treated at 500 °C.**Fig. 1.** SEM micrographs for TiO<sub>2</sub>-DAPs and zeolite/DAP hybrids: (a) TiO<sub>2</sub>-DAPs, (b) Z2/DAP, (c) Z3/DAP and (d) Z5/DAP.

of existing particles (surface oxidation pathway) or transformation of DAPs to crystals containing high-index facets could explain the formation of these deposits. The freezing-drying technique to incorporate DAPs on the zeolitic materials, keep the typical morphologies of raw DAPs. The commercial TiO<sub>2</sub> particles are spherical and have lower particle size than DAPs, around 10–20 nm, forming irregular clusters, in line with previous reports [19]. Fig. 1**b–d**, show representative SEM images for Z2/DAP, Z3/DAP and Z5/DAP samples, respectively. The DAPs structure in the APHs is maintained with a main particle size of 100 nm and particles can be distinguished easily from the zeolite phase. Fig. 1**b** shows zeolite Y particles of sizes between 400 and 700 nm, mixed with decahedral anatase particles. The Z3/DAP containing ZSM-5 zeolite with a SiO<sub>2</sub>/Al<sub>2</sub>O<sub>3</sub> ratio of 23 (Fig. 1**c**), is also characterized by crystals

of around 400–700 nm with similar DAPs dispersion than Z2/DAP. The morphology of the Z5 (ZSM-5 SiO<sub>2</sub>/Al<sub>2</sub>O<sub>3</sub> 280) Fig. 1**d**, is characterized by irregular zeolites particles with considerable higher particle size than the others zeolites, ranging from 700 nm to 1 μm and a large dispersion of DAPs can be appreciated. Therefore, the results seem to indicate that ZSM-5 with high SiO<sub>2</sub>/Al<sub>2</sub>O<sub>3</sub> improves the dispersion of TiO<sub>2</sub> respect to the others zeolites, favouring the adsorption of UV irradiation for a higher fraction of titania particles decorating the surface. Thus, the selection of the zeolite with the adequate composition and crystal structure plays a relevant role in the control and improvement of the dispersion of DAPs.

Fig. 2 shows the X-ray patterns for DAPs and zeolite/DAP hybrids. TiO<sub>2</sub>-anatase phase (JCPDS 89-4921) is the main TiO<sub>2</sub> phase detected in the samples. TiO<sub>2</sub>-rutile phase (JCPDS 87-0920) is

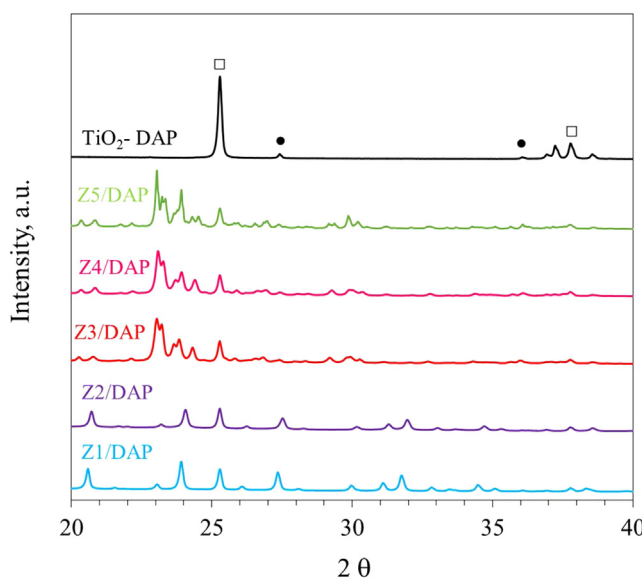


**Fig. 2.** X-ray diffractograms of  $\text{TiO}_2$ -DAPs and zeolite/DAP hybrids: (□)  $\text{TiO}_2$ -anatase and (●)  $\text{TiO}_2$ -rutile.

also observed as a minority component. The characteristic diffraction lines for the MFI (Z3, Z4 and Z5) and FAU (Z1 and Z2) zeolites along with the peaks for  $\text{TiO}_2$ -anatase phase are observed in the diffractograms of the zeolite/DAP hybrids. As deduced by the well-defined, very intense and small breadth diffraction peaks, the zeolites are highly crystalline [39]. The intensity of the diffraction peaks of the zeolite phases decreases after the mixing with  $\text{TiO}_2$  due to a dilution effect [40]. Peaks from the  $\text{TiO}_2$ -rutile crystal phase are not detected in the hybrid materials. Quantitative determination of the ratio of {001}/{101} facets areas are, at present, rather difficult due to possible heterogeneity of particles. Aspect-ratio estimation seems one of possible comprehensive methods to calculate the proportion of {101}-plane exposure. Particle Aspect Ratio (PAR) was evaluated, for convenience, as a ratio of crystallite size (depth) vertical to {001} and {101} lattice planes ( $d_{004}$  and  $d_{101}$ , respectively) calculated using Scherrer's equation [41]; the higher the aspect ratio is, the higher is the proportion of {101}-plane exposure. Thus, the PAR parameter was estimated to be 0.8–0.9, indicating that more than 80% of total surface corresponds to {101} facets for the decahedral particles prepared in this study. These data are in line with those reported in the literature [41]. According to XRD, DAP are well crystalized (c.a. > 90%). The main crystal phase detected was  $\text{TiO}_2$ -anatase (c.a. 87.9%) and a minor proportion of  $\text{TiO}_2$ -rutile (5.9%). The amorphous phase content at the selected synthesis conditions was lower than 5.0%. Anatase titania particles showed a mean crystal size of ca. 67 nm comparing to only 15 nm for commercial  $\text{TiO}_2$ . Larger DAPs showed high stability due to the presence of  $\text{OH}^-$  and  $\text{OH}^+$  adsorbed groups [8].

UV-vis diffuse reflectance spectra of DAPs, zeolite/DAP composites and commercial  $\text{TiO}_2$  as a reference was evaluated (Figure not shown). The spectra for the zeolites were featureless indicating the lack of absorption. On the other hand, the hybrids containing  $\text{TiO}_2$ -DAPs showed an absorption edge at around 380 nm. The band gap was calculated by plotting the modified Kubelka-Munk function,  $(F(R_\infty)E)^{0.5}$  versus the energy of the exciting light, determining the band gap [42]. The band gap energy value was between 3.0 for DAP based materials and 3.2 eV for the ones based on  $\text{TiO}_2$ -G5, consistent with the characteristic value reported in the literature for  $\text{TiO}_2$  [4]. The UV absorption band gap of  $\text{TiO}_2$  is affected by the exposed facets following the order: {010} > {101} > {001} [7]. Thus, the blue

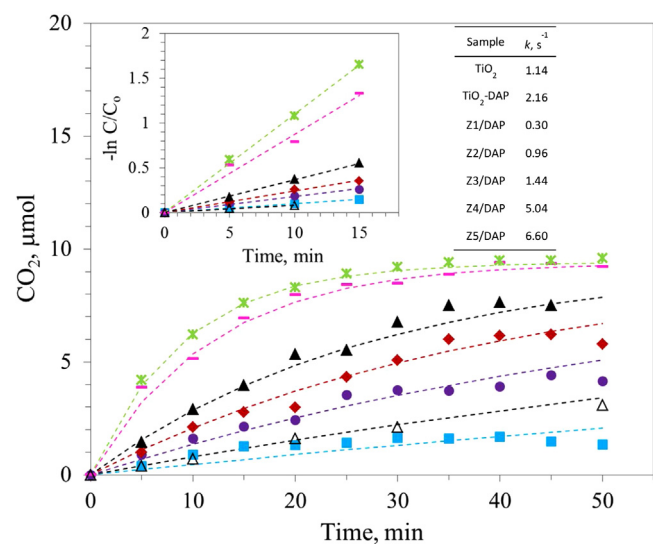


**Fig. 3.** Amount of  $\text{CO}_2$  generated during the acetaldehyde photodegradation in air: (Δ) commercial  $\text{TiO}_2$ , (▲)  $\text{TiO}_2$ -DAPs, (■) Z1/DAP, (●) Z2/DAP, (◆) Z3/DAP, (▼) Z4/DAP and (★) Z5/DAP. Dashed lines: theoretical curves assuming a first order reaction. Operation conditions: reactor volume:  $V = 114 \text{ mL}$ ,  $[\text{CH}_3\text{CHO}] = 1,000 \text{ ppm}$ -ca. 5  $\mu\text{mol}$ ,  $\text{g}_{\text{TiO}_2} = 6.4 \text{ mg}$ .

shift observed for  $\text{TiO}_2$ -DAPs, was related to the present of {001} facets.

### 3.2. Photocatalytic activity of hybrid materials

Firstly, the photocatalytic activity of the zeolite/DAP hybrids and of the reference titania materials was studied in a batch reactor. Fig. 3 shows the rate of  $\text{CO}_2$  formation during acetaldehyde decomposition as function of the irradiation time with  $\text{TiO}_2$ -DAPs and zeolite/DAPs. Irrespectively of the catalysts under study,  $\text{CO}_2$  formation increases with reaction time.

The mineralization (total oxidation) of one mole of acetaldehyde produces two moles of  $\text{CO}_2$  ( $\text{CH}_3\text{CHO} + 5/2\text{O}_2 \rightarrow 2\text{CO}_2 + 2\text{H}_2\text{O}$ ). As observed in Fig. 3, the amount of  $\text{CO}_2$  obtained during the mineralization of  $\text{CH}_3\text{CHO}$  is lower than the stoichiometric value except with Z5/DAP. This behaviour indicates that intermediate species are formed with the other catalysts or that the reaction products remain adsorbed on the composites [43]. Thus, the Z5/DAP hybrid is the only one endowed with enough activity to mineralize the initial amount of AcH. Pure  $\text{TiO}_2$ -DAPs reaches a  $\text{CH}_3\text{CHO}$  conversion of 73% meanwhile only a 22% was attained with the commercial  $\text{TiO}_2$ . Any of the microporous materials tested showed photocatalytic activity for the degradation of this compound for themselves.

The variation of the zeta potential with the pH for suspension of commercial  $\text{TiO}_2$  and DAPs was analyzed (Figure not shown). The isoelectric point (IEP) indicates the pH at which the positive ( $-\text{OH}_2^+$ ) and negative ( $-\text{O}^-$ ) surface charges are in average.  $\text{TiO}_2$ -G5 and DAPs suspension present an IEP point at pH of 5.9 and 6.5 respectively. These results suggest that the average acid strength of surface hydroxyl is in the order of  $\text{TiO}_2$ -G5 > DAP probably related to the presence of {001} facet on the later [44]. All the studied zeolites present an isoelectric point at pH lower than two, except zeolite Z1 which exhibits an isoelectric point at pH = 7. The preparation of the hybrid was performed in water at pH between 6.5 – 7. At this pH, near the isoelectric point of both materials, with the same positive and negative net charges, the interaction between  $\text{TiO}_2$  and zeolite Y Z1 is prevented, explaining the low photoactivity of the Z1/DAP.

The apparent rate constants for each photocatalyst have been calculated (Fig. 3 inset). The value for the synthesized DAP was twice than that of commercial  $\text{TiO}_2$  ( $2.16 \text{ s}^{-1}$  vs.  $1.14 \text{ s}^{-1}$ ). It is worth

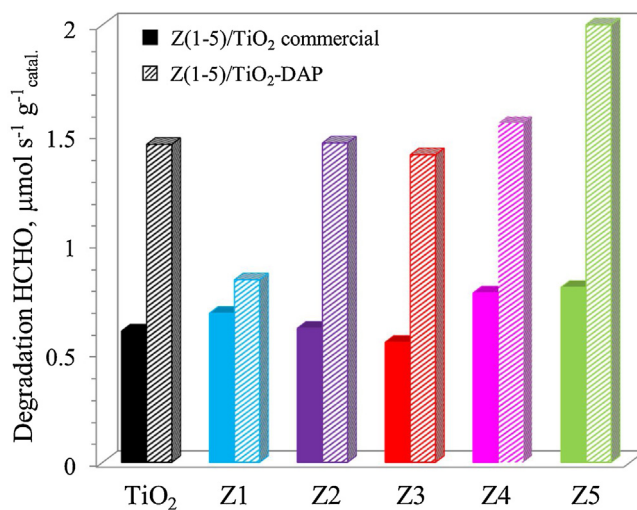


**Fig. 4.** Photocatalytic degradation rate of formaldehyde in air with UV-A irradiation for TiO<sub>2</sub> and zeolite/TiO<sub>2</sub> hybrids: (filled bars) Zeolite/TiO<sub>2</sub>-G5 and (hatched bars) zeolite/TiO<sub>2</sub>-DAP samples. Operating conditions: total flow F=900 mL min<sup>-1</sup>, [HCHO]=15 ppm, tr=0.43 s (residence time) and g<sub>catal</sub>=30 mg.

nothing to remark the values obtained for ZSM-5 based materials with high SiO<sub>2</sub> content, where this value increases up to 6.6 s<sup>-1</sup>. Moreover, the experimental data have been fitted to the theoretical data, assuming a first order integrated rate equation, which relates the apparent rate constant (*k*) with the concentration of AcH (Eq. (2)):

$$C = C_0(1 - \exp(-kt)) \quad (2)$$

Where *C* is the amount of CO<sub>2</sub> produced and *C*<sub>0</sub> is the initial concentration of acetaldehyde and *t* is the reaction time (dash lines in Fig. 3). The theoretical curves fit well with the experimental points, indicating that the photocatalytic degradation of acetaldehyde depends linearly on the amount of acetaldehyde. This behaviour is commonly observed for gas-phase reactions at low concentration of reactants. Nevertheless, the adsorption and the diffusional processes on the composites, should be considered in order to explain the reaction rate results obtained. Since DAPs surface area is relative low, the higher rate constants for zeolite/DAP composites may show that the adsorption/diffusion of acetic acid on the zeolites but not on DAPs, enhances the reaction rate.

As observed, zeolite/DAP photocatalysts show higher AcH mineralization than commercial TiO<sub>2</sub>, except Z1/DAP. ZSM-5 with high silica content and high dispersion of the titania, enhances the photocatalytic activity of the bare DAPs, reaching conversions around 95%. In good agreement with previous reports, the photocatalytic activity increases with the hydrophobic character of the zeolite, especially for those with the MFI structure [18]. Shape-controlled anatase titanium(IV) oxide particles were synthetized by hydrothermal treatment of peroxytitanic acid (PTA) solution with polyvinyl alcohol as a shape-control reagent and tested in the photodegradation of acetaldehyde [12]. A 60% of acetaldehyde conversion was achieved after 100 min reaction time. Sugishita et al. studied the photodegradation of DAPs for AcH removal, in a similar experimental set up to the ones used in this study [13]. Authors report a 40% AcH conversion after 60 min of reaction time. The hybrid of our study based on ZSM-5 with only an 8wt% of DAPs allows more than 90% AcH conversion at similar reaction time.

In order to test the catalytic properties of the zeolite/DAP under harsh conditions the degradation of HCHO was studied. For this purpose, a continuous air flow was fed through the photocatalytic reactor, without recirculation, changing the total gas flow from 500 to 900 mL min<sup>-1</sup> (GHSV=4,600 – 8,000 h<sup>-1</sup>). According to the fol-

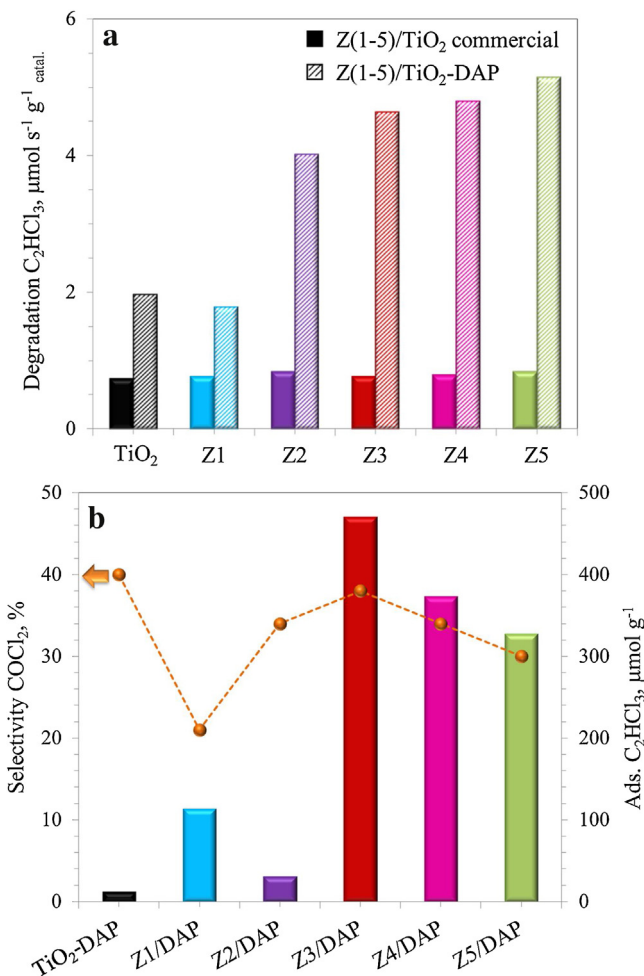


**Fig. 5.** Photocatalytic degradation of trichloroethylene in air with UV-A irradiation for TiO<sub>2</sub> and zeolite/TiO<sub>2</sub> hybrids: (a) Degradation rate of C<sub>2</sub>HCl<sub>3</sub>: (Filled bars) zeolite/TiO<sub>2</sub>-G5, (hatched bars) zeolite/DAPs and (b) Relationship between COCl<sub>2</sub> selectivity and adsorption ability: (●) COCl<sub>2</sub> selectivity and (filled bars) amount of C<sub>2</sub>HCl<sub>3</sub> adsorbed. Operating conditions: total flow F=700 mL min<sup>-1</sup>, [C<sub>2</sub>HCl<sub>3</sub>]=25 ppm, tr=0.56 s residence time and g<sub>catal</sub>=30 mg.

lowing equation HCHO + O<sub>2</sub> → CO<sub>2</sub> + H<sub>2</sub>O, the total oxidation of one mole of HCHO produces one mole of CO<sub>2</sub>. Fig. 4 shows the degradation rate of formaldehyde, for all catalysts. As observed, the rate of HCHO degradation on TiO<sub>2</sub>-DAPs was 2.4 times higher than that on TiO<sub>2</sub>-G5. DAPs with a PAR ratio of 0.8-0.9 result in a two-fold increase of the VOC photodegradation rate with respect to that of benchmark TiO<sub>2</sub> under both static and dynamic conditions. As observed in Fig. 4, the HCHO degradation follows the same trend as observed before for the CH<sub>3</sub>CHO degradation with the Z1-Z5 based photocatalysts. The hybrid photocatalysts prepared with DAP showed notably better photocatalytic performances than those based on commercial TiO<sub>2</sub> specially for Z5/DAP. The improvement of the photocatalytic efficiency was related to the high crystallinity and low density of defects of DAPs with {001} facets [5]. The presence of {001} facets promotes a selective migration and separation of electrons and positive holes and enhanced the photocatalytic oxidation paths in combination with a most thermodynamically stable {101} facets [45,46].

Finally, the composites were tested in the photodegradation of an organochloride compound such as trichloroethylene (TCE). The photocatalytic degradation pathway of this molecule is complex, resulting in the formation of a large quantity of reaction intermediates, along with non-desired products. In addition to the formation of CO<sub>2</sub> and HCl, TCE degradation also leads to the formation of

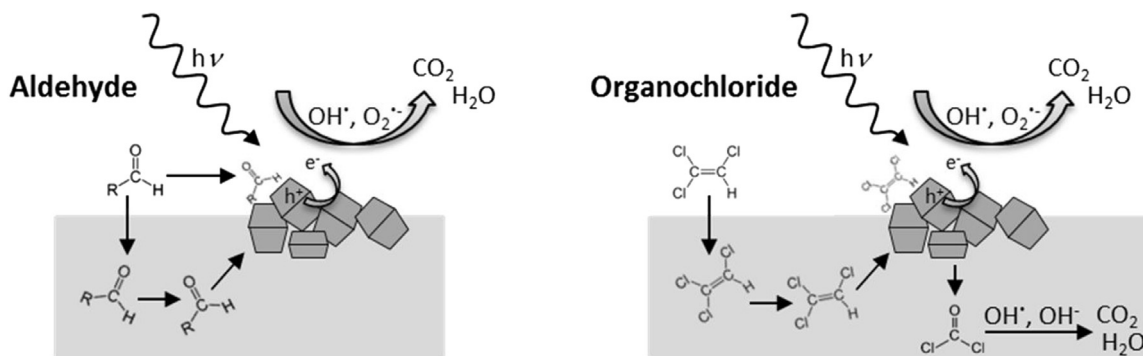


**Fig. 6.** Scheme for aldehyde (left) or organochloride (right) photooxidation with zeolite/DAP hybrids. Zeolitic material (■) and DAPs particles (□).

significant amounts of harmful products such as dichloroacetyl chloride (DCAC),  $\text{COCl}_2$  and CO [47]. Fig. 5a shows the degradation rate of TCE with the hybrids materials prepared with commercial  $\text{TiO}_2$  and DAP. Again, the hybrids containing DAPs are more efficient for the removal of TCE than those prepared with commercial titania, in spite of the different surface area. The differences between the photocatalytic performance of DAPs and commercial  $\text{TiO}_2$  is accentuated when the zeolite is included in the photocatalytic system, this is, degradation rates are higher when the zeolite is mixed with  $\text{TiO}_2$ . The activity pattern described for the effect of the  $\text{SiO}_2/\text{Al}_2\text{O}_3$  ratio for the oxidation of  $\text{HCHO}$  and  $\text{CH}_3\text{CHO}$  is also observed during the degradation of TCE. The conversion of TCE with Z5/DAP at  $700 \text{ mL min}^{-1}$  is 63% while  $\text{TiO}_2$ -DAP reaches only a 50% conversion. Fig. 5b shows the selectivity to  $\text{COCl}_2$  which along with  $\text{CO}_2$  are the main products detected and the amount of TCE adsorbed on the hybrid catalysts. We have also observed that the photocatalysts prepared with the zeolites with higher silica contents result in both higher degradation rates and a 12% lower production of  $\text{COCl}_2$  with respect to that obtained with DAPs. The results indicate an inverse relationship between the selectivity to  $\text{COCl}_2$  and the adsorption capacity. The photocatalytic properties of  $\text{TiO}_2$ -DAPs in the degradation of this molecule have not been reported in the literature. Previous results obtained in our group with hybrid materials based on sepiolite (a natural magnesium silicate) and commercial  $\text{TiO}_2$  indicate at least four times higher reaction rate for zeolite/DAP respect to the magnesium silicate based material [15]. In the case of Z5/DAP composite, values of  $5.10 \mu\text{mol s}^{-1} \text{ g}^{-1}_{\text{catal.}}$  vs.  $0.41 \mu\text{mol s}^{-1} \text{ g}^{-1}_{\text{catal.}}$  for Sep/ $\text{TiO}_2$  at  $700 \text{ mL min}^{-1}$  were obtained. Beside the intrinsic properties of DAPs, the combination of the adsorption properties of the zeolitic structures, along to its hydrophobic nature and the improvement of the dispersion of semiconductor on the microporous material, are key factors to explain the results.

Our results indicate a direct relationship between the amount of VOC adsorbed and aluminium content of the microporous material and the formation of undesirable products. Takeuchi et al. reported a similar effect and concluded that if the strength of adsorption of the reactant molecules with the zeolite is strong, they cannot diffuse toward the  $\text{TiO}_2$  surface whereas molecules weakly adsorbed on the zeolite surface can easily diffuse toward the  $\text{TiO}_2$  surfaces, resulting in an enhancement of the photocatalytic reactivity [26]. Therefore, to select the adequate adsorbent to be combined with the  $\text{TiO}_2$  it is important to consider the adsorption ability and the strength of the interaction, so that the diffusion of the adsorbent towards the semiconductor is not impeded. Hybrid materials prepared with ZSM-5 with high silicon content combined to DAPs allow an improvement of the VOC photodegradation rate favouring the mineralization process. The improvement of the photocatalytic degradation of the VOC with zeolite/DAPs is related to the combination of a moderate adsorption strength of the gas molecule onto

the zeolite and the direct and indirect diffusion of the pollutant and reaction products from the zeolite to  $\text{TiO}_2$ -DAPs active sites and from the titania to the adsorbent. Moreover, the presence of {001} facets and the high crystallinity of the  $\text{TiO}_2$ -DAPs reduces the electron and hole recombination reactions, thus improving photooxidation pathways.

Two different mechanisms may be proposed depending on the nature of pollutant to be treated (Fig. 6): For aldehydes (FMD or AcH) which are adsorbed on both phases,  $\text{TiO}_2$  and zeolitic material, and no reaction products others than  $\text{CO}_2$  are produced, the role of the microporous material is buffer the access of the aldehyde to the active sites. Then, the photocatalytic process occurs, involving the radical species ( $\text{OH}^\cdot$  and  $\text{O}_2^{\cdot-}$ ) generated on DAPs {101} and {010} facets (Fig. 6 left).

For the organochloride compound, which is preferentially adsorbed on the microporous materials, a migration of the pollutant from the zeolite to the  $\text{TiO}_2$  active sites is produced, where the photocatalytic process occurs (Fig. 6 right). Moreover, non-desirable reaction products may migrate again into the zeolitic structure, where they are either retained or suffer further hydrolysis reaction. Migration of radical species generated on the titania active sites for long distances on siliceous materials, has been reported in the literature [48]. Thus, this reaction pathway cannot be ruled out. Further experiments are being carried out in our laboratory to elucidate the different reaction pathways.

#### 4. Conclusions

DAPs with well-defined {101} and {001} facets, prepared by gas phase reaction at high temperature, were immobilized on different types of zeolites by the freezing-drying technique. Zeolite/DAP hybrids are efficient photocatalysts for the degradation of different types of aldehydes and organochloride compounds in gas phase both in batch and continuous flow reactors. Zeolite/DAP hybrids, combine the intrinsic properties of the raw materials, resulting in low BET area of the composites, the blocking of a small fraction of micropores and a modification of the amount of VOC adsorbed, preserving the zeolite and DAPs morphology and crystallinity. The nature of the zeolite has a strong influence on the adsorption properties and on the dispersion of DAPs. The isoelectric point of microporous material is a key parameter that determines the dispersion of titania particles.

DAPs with a particle aspect ratio of 0.8–0.9 result in a two-fold increase of the VOC photodegradation reaction rate with respect to that of benchmark  $\text{TiO}_2$  under both static and dynamic conditions. Zeolite/DAP hybrids have higher photocatalytic properties than those prepared with commercial  $\text{TiO}_2$ . The amount of VOC adsorbed is promoted on the high aluminium containing zeolites. Nevertheless, hybrid materials prepared with zeolites with high silicon content, especially ZSM-5, lead to an enhancement of the

photodegradation rate favouring the mineralization process. The improvement of the photocatalytic efficiency with zeolite/DAPs is related to the combination of a moderate adsorption strength of the VOC onto the zeolite and the direct and indirect diffusion of the pollutant and reaction products from the zeolite to the TiO<sub>2</sub>-DAPs active sites and from the titania to the adsorbent. Moreover, the presence of {001} facets and the high crystallinity of the TiO<sub>2</sub>-DAPs reduces the electron-hole recombination reactions, thus improving photooxidation pathways.

## Acknowledgment

The authors acknowledge the Spanish Ministry of Economy and Competitiveness and European Union for the financial support (projects CTM-2011-25093 and LIFE12-ENV.ES.000280); Ms. Jansson thanks the Spanish Ministry for the PhD grant (BES-2012-055758 and EEBB-I-1408837). Authors are grateful to Dr. R. Campos for the N<sub>2</sub> adsorption-desorption analysis.

## References

- [1] M.R. Hoffmann, S.T. Martin, W. Choi, D.W. Bahnemann, *Chem. Rev.* 95 (1995) 69–96.
- [2] A. Wold, *Chem. Mater.* 5 (1993) 280–283.
- [3] J.L. Gole, J.D. Stout, C. Burda, Y. Lou, X. Chen, *J. Phys. Chem. B* 108 (2004) 1230–1240.
- [4] A.L. Linsebigler, L. Guangquan, J.T.J. Yates, *Chem. Rev.* 95 (1995) 735–758.
- [5] F. Amano, O.-O. Prieto-Mahaney, Y. Terada, T. Yasumoto, T. Shibayama, B. Ohtani, *Chem. Mater.* 21 (2009) 2601–2603.
- [6] H.G. Yang, C.H. Sun, S.Z. Qiao, J. Zou, G. Liu, S.C. Smith, H.M. Cheng, G.Q. Lu, *Nature* 453 (2008) 638–641.
- [7] J. Pan, G. Liu, G.Q. Lu, H.-M. Cheng, *Angew. Chem. Int. Ed. Engl.* 50 (2011) 2133–2137.
- [8] M. Janczarek, E. Kowalska, B. Ohtani, *J. Chem. Eng.* 289 (2016) 502–512.
- [9] M. Dozzi, E. Selli, *Catalysts* 3 (2013) 455–485.
- [10] K. Lv, B. Cheng, J. Yu, G. Liu, *Phys. Chem. Chem. Phys.* 14 (2012) 5349–5362.
- [11] I.A. Perales-Martínez, V. Rodríguez-González, S. Obregon-Alfaro, S.W. Lee, J. Nanosci. Nanotechnol. 15 (2015) 7351–7356.
- [12] N. Murakami, Y. Kurihara, T. Tsubota, T. Ohno, *J. Phys. Chem. C* 113 (2009) 3062–3069.
- [13] N. Sugishita, Y. Kuroda, B. Ohtani, *Catal. Today* 164 (2011) 391–394.
- [14] F. Fresno, R. Portela, S. Suárez, J.M. Coronado, *J. Mater. Chem. A* 2 (2014) 2863–2884.
- [15] S. Suárez, J.M. Coronado, R. Portela, J.C. Martín, M. Yates, P. Ávila, B. Sánchez, *Environ. Sci. Technol.* 42 (2008) 5892–5896.
- [16] T.L.R. Hewer, S. Suárez, J.M. Coronado, R. Portela, P. Avila, B. Sanchez, *Catal. Today* 13 (2009) 302–308.
- [17] S. Suárez, T.L.R. Hewer, R. Portela, M.D. Hernandez-Alonso, R.S. Freire, B. Sanchez, *Appl. Catal. B* 101 (2011) 176–182.
- [18] I. Jansson, S. Suárez, F.J. García-García, B. Sánchez, *Appl. Catal. B* 178 (2015) 100–107.
- [19] R. Portela, I. Jansson, S. Suárez, M. Villarroel, B. Sánchez, P. Avila, *Chem. Eng. J.* (2016) (in press).
- [20] A. Corma, H. Garcia, *Chem. Commun.* 13 (2004) 1443–1459.
- [21] L. Shirazi, E. Jamshidi, M.R. Ghasemi, *Cryst. Res. Technol.* 43 (2008) 1300–1306.
- [22] X. Du, E. Wu, *J. Phys. Chem. Solids* 68 (2007) 1692–1699.
- [23] S. Zhang, N. Fujii, Y. Nosaka, *J. Mol. Catal. A: Chem.* 129 (1998) 219–224.
- [24] K. Hashimoto, K. Wasada, M. Osaki, E. Shono, K. Adachi, N. Toukai, H. Kominami, Y. Kera, *Appl. Catal. B* 30 (2001) 429–436.
- [25] Y. Kuwahara, H. Yamashita, *J. Mater. Chem.* 21 (2011) 2407–2416.
- [26] M. Takeuchi, M. Hidaka, M. Anpo, *J. Hazard. Mater.* 237–238 (2012) 133–139.
- [27] E. Grabowska, M. Diak, M. Marchelek, A. Zaleska, *Appl. Catal. B* 156–157 (2014) 213–235.
- [28] F. Izumi, K. Momma, *Solid State Phenom.* 130 (2007) 15–20.
- [29] J. Tauc, *Mater. Res. Bull.* 5 (1970) 721–729.
- [30] I. Jansson, K. Yoshiiri, H. Hori, F.J. García-García, S. Rojas, B. Sánchez, B. Ohtani, S. Suárez, *Appl. Catal. A* 521 (2016) 208–219.
- [31] S. Suárez, N. Arconada, Y. Castro, J.M. Coronado, R. Portela, A. Durán, B. Sánchez, *Appl. Catal. B* 108–109 (2011) 14–21.
- [32] G. Leofanti, M. Padovan, G. Tozzola, B. Venturelli, *Catal. Today* 41 (1998) 207–219.
- [33] J. Weitkamp, *Solid State Ionics* 131 (2000) 175–188.
- [34] H. Yamashita, H. Li, *Nanostructured Photocatalysts: Advanced Functional Materials*, Springer International Publishing, Switzerland, 2016.
- [35] K.D. Dubois, A. Petushkov, E. Garcia Cardona, S.C. Larsen, G. Li, *J. Phys. Chem. Lett.* 3 (2012) 486–492.
- [36] X.S. Zhao, Q. Ma, G.Q. Lu, *Energ. Fuel.* 12 (1998) 1051–1054.
- [37] N.Y. Chen, *J. Phys. Chem.* 80 (1976) 60–64.
- [38] T. Noguchi, A. Fujishima, K. Hashimoto, P. Sawunyama, *Environ. Sci. Technol.* 32 (23) (1998) 3831–3833.
- [39] D.P. Serrano, G. Calleja, J.A. Botas, F.J. Gutierrez, *Sep. Purif. Technol.* 54 (2007) 1–9.
- [40] A.H. Alwash, A.Z. Abdullah, N. Ismail, *World Acad. Sci. Eng. Technol.* 7 (2013) 375–383.
- [41] B. Ohtani, *Chem. Lett.* 37 (2008) 216–229.
- [42] K.A. Michalow, D. Logvinovich, A. Weidenkaff, M. Amberg, G. Fortunato, A. Heel, T. Graule, M. Rekas, *Catal. Today* 144 (2009) 7–12.
- [43] I. Sopyan, M. Watanabe, S. Murasawa, K. Hashimoto, *J. Photochem. Photobiol. A* 98 (1996) 79–86.
- [44] F. Amano, T. Yasumoto, O.O.P. Mahaney, S. Uchida, T. Shibayama, Y. Terada, B. Ohtani, *Top. Catal.* 53 (2010) 455–461.
- [45] M. Maisano, M.V. Dozzi, M. Coduri, L. Artiglia, G. Granozzi, E. Selli, *Appl. Mater. Interfaces* 8 (2016) 9745–9754.
- [46] B. Ohtani, *Catalysts* 3 (2013) 942–953.
- [47] M.D. Driessens, T.M. Miller, V.H. Grassian, *J. Mol. Catal. A: Chem.* 131 (1998) 149–156.
- [48] H. Haick, Y. Paz, *J. Phys. Chem. B* 105 (2001) 3045–3051.